Numerical Investigation of Sediment Transport of Sandy Beaches by a Tsunami-Like Solitary Wave Based on Navier–Stokes Equations

Article *in* Journal of Nondestructive Evaluation Diagnostics and Prognostics of Engineering Systems · April 2019

DOI: 10.1115/1.4043504

CITATIONS
6

READS
199

7 authors, including:

Cheng Liu
Pearl river hydraulic research institute, Guangzhou,China
8 PUBLICATIONS **25** CITATIONS
SEE PROFILE

Xiaojian Liu
Pearl River Hydraulic Research Institute
19 PUBLICATIONS **151** CITATIONS
SEE PROFILE

Zhiyuan Wu
Changsha University of Science and Technology
38 PUBLICATIONS **333** CITATIONS
SEE PROFILE

Journal of Offshore Mechanics and Arctic Engineering

CURRENT ISSUE

December 2019, Volume 141, Issue 6

View This Issue

ISSUES IN PROGRESS

Volume 142, Issue 2, April 2020

Volume 142, Issue 1, February 2020

About the Journal

The *Journal of Offshore Mechanics and Arctic Engineering* is an international resource for original peer-reviewed research that advances the state of knowledge on all aspects of analysis, design, and technology development in ocean, offshore, arctic, and related fields. Read more...

Lance Manuel,
University of Texas at Austin
View Full Editorial Board

Impact Factor
1.133

Cheng Liu
Pearl River Hydraulic Research Institute,
Pearl River Water Resources Commission of the
Ministry of Water Resources,
Guangzhou, Guangdong 510611, China
e-mail: jacklc2004@163.com

Xiaojian Liu[1]
Pearl River Hydraulic Research Institute,
Pearl River Water Resources Commission of the
Ministry of Water Resources,
Guangzhou, Guangdong 510611, China;
School of Hydraulic Engineering,
Changsha University of Science and Technology,
Changsha, Hunan 410114, China;
School of Civil Engineering,
Sun Yet-Sen University,
Guangzhou, Guangdong 510611, China
e-mail: lxiaojian2010@163.com

Changbo Jiang
School of Hydraulic Engineering,
Changsha University of Science and Technology,
Changsha, Hunan 410114, China
e-mail: jiangchb@csust.edu.cn

Yong He
Pearl River Hydraulic Research Institute,
Pearl River Water Resources Commission of the
Ministry of Water Resources,
Guangzhou, Guangdong 510611, China
e-mail: heyongwhu@126.com

Bin Deng
School of Hydraulic Engineering,
Changsha University of Science and Technology,
Changsha, Hunan 410114, China
e-mail: dengbin07@csust.edu.cn

Zihao Duan
Key Laboratory of Ecosystem Network Observation
and Modeling,
Institute of Geographic Sciences and Natural
Resources Research,
Chinese Academy of Sciences,
Beijing 100101, China
e-mail: duanzh.18b@igsnrr.ac.cn

Zhiyuan Wu
School of Hydraulic Engineering,
Changsha University of Science and Technology,
Changsha, Hunan 410114, China
e-mail: zwu@csust.edu.cn

Numerical Investigation of Sediment Transport of Sandy Beaches by a Tsunami-Like Solitary Wave Based on Navier–Stokes Equations

To improve our current understanding of tsunami-like solitary waves interacting with sandy beach, a nonlinear three-dimensional numerical model based on the computational fluid dynamics (CFD) tool OpenFOAM® is first self-developed to better describe the wave propagation, sediment transport, and the morphological responses of seabed during wave runup and drawdown. The finite volume method (FVM) is employed to discretize the governing equations of Navier–Stokes equations, combining with an improved volume of fluid (VOF) method to track the free surface and a k–ε model to resolve the turbulence. The computational capability of the hydrodynamics and the sediment transport module is well calibrated by laboratory data from different published references. The results verify that the present numerical model can satisfactorily reproduce the flow characteristics, and sediment transport processes under a tsunami-like solitary wave. The water-sediment transport module is then applied to investigate the effects of prominent factors, such as wave height, water depth, and beach slope, in affecting the beach profile change. Finally, a dimensionless empirical equation is proposed to describe the transport volume of onshore sediment based on simulation results, and some proper parameters are recommended through the regression. The results can be significantly helpful to evaluate the process of transported sediment by a tsunami event. [DOI: 10.1115/1.4043504]

Keywords: solitary wave, Navier–Stokes equations, sandy beach, sediment transport

1 Introduction

Tsunami is a giant devastating wave created by the undersea earthquake, volcanic eruptions, plate movement, or landslide and generally defined as long period waves (of the order of hundreds to thousands of seconds). As the tsunami wave gets closer to coastal areas, the wave height may increase dramatically along with the disastrous potential destruction. Examples of such destructive hazard could be witnessed around the coasts of the Indian Ocean on Dec. 26, 2004 [1] and the Japan coasts on Mar. 11, 2011 [2], which caused massive devastation and loss of life. Field surveys showed that in addition to hydrodynamic and debris impact, tsunamis can also erode the coastlines and the soil supporting structural foundations and roadways [3].

Due to the devastating scouring effect of tsunami waves, assessing the sediment transport process is important to infer the intensity of past tsunamis and tsunami hazards [4]. Many examples of

[1]Corresponding author.

Contributed by the Ocean, Offshore, and Arctic Engineering Division of ASME for publication in the Journal of Offshore Mechanics and Arctic Engineering. Manuscript received October 15, 2018; final manuscript received April 2, 2019; published online May 9, 2019. Assoc. Editor: Xinshu Zhang.

tsunami deposits have been reported from coastal areas. For example, by analyzing grain-size distribution, coastal retreat, and field videos, researchers indicated that the majority of the deposit sources are from the beach and not from the deep ocean floor (e.g., [3,5]), as well as both runup and drawdown contribute to the deposits (e.g., [6,7]). Over the last few decades, although our understanding of the tsunami-induced erosion and deposition mechanisms has improved substantially, the majority of previous studies are still needed to reconstruct the tsunami flow characteristics from the deposited records. In addition, it could raise a considerably limited information on tsunami-induced instantaneously sediment transport mechanisms due to frequent lack of local wave condition and topography, especially when face complicated three-dimensional effects from wave–structure interactions. Hence, physical experiments and numerical simulations could provide effective controlling factors that are required for improving the understanding of these processes.

In the literature, the interactions between the regular/irregular wave and the sandy beach were studied by many researchers experimentally (e.g., [8,9]), numerically (e.g., [10,11]), theoretically (e.g., [12,13]), and observationally (e.g., [14,15]). However, tsunami waves are different from the regular/irregular waves in their magnitudes and dispersive properties. Thus, for the erosion and deposition processes of the sandy beach exposed to tsunami waves, the knowledge about the morphological responses need to be further studied to guide future development of coastlines and coastal infrastructures in those coastal areas where the occurrence of earthquake-induced tsunami is not rare. Solitary wave has been employed in many related studies to model the leading tsunami wave because the former can represent many important properties of the latter [16]. Traditionally, experimental studies can be significantly helpful to evaluate the process of transported sediment by the tsunami wave. Kobayashi and Lawrence [17] performed a series of physical experiments to examine the cross-shore sediment transport processes under breaking solitary waves on a fine sand beach. The initial beach slope of 1/12 was exposed to a positive solitary wave eight times. Moronkeji and Rolla [18] have conducted physical experiments on the runup and drawdown of the solitary wave over a movable bed at two different beach slopes. Tsujimoto et al. [19] examined the beach profile changes under solitary waves alone and in combination with regular waves. Young et al. [20] investigated the erosion and deposition patterns under breaking positive solitary waves and found that tsunami runup and drawdown could cause liquefaction failure of coastal fine sand slopes due to the generation of high excess pore pressure. Jiang et al. [21] presented the bed load transport formulas for the tsunami up rush and backwash processes based on the laboratory experiments. Daghighi et al. [22] experimentally assessed the sediment transport and bed formation of sandy beaches by tsunami waves and put forward an empirical formula to describe the transported sediment volume. In addition to laboratory experiments, the numerical model provided us an alternative way to understand the mechanics because of the limited capability of measurement devices used in physical experiments and field observations. Modeling interactions between waves and sandy beach have been studied by many researchers in the past with depth-averaged models, such as the shallow water equations (e.g., [23,24]) and the Boussinesq-type equations (e.g., [25,26]). However, the wave and sandy beach interaction problem is highly nonlinear, local, but strong turbulence near the seabed and the free surface needs to be considered. Recently, Nakamura and Yim [27] adopted a volume of fluid (VOF) type model that was based on the generalized Navier–Stokes equations, the large eddy simulation (LES) turbulence closure solver to compute incompressible viscous multiphase flows, and the finite difference method to discretize computational space. This model is applied to predict the cross-shore profile change of a sloping beach due to breaking solitary waves and found that it can predict reasonably well the sediment transport and the resulting beach profile change compared with the measured data from a set of hydraulic tests. However, some mechanisms of this process, such as the beach profile change and the corresponding sediment transport volume during a tsunami-like solitary wave event, which be rooted in the complex hydrodynamic and sandy conditions, are still unknown and should be clearly and rigorously stated.

To remedy the deficiency of current understanding in aforementioned problems, we employed a three-dimensional (3D) numerical model developed under OpenFOAM (open field operation and manipulation) in this study. OpenFOAM is a widely used open-source computational fluid dynamics code supporting two-phased incompressible flow. Recently, it has become a powerful and efficient tool to simulate nearshore wave dynamics via its solver interFoam combined with wave generation and absorption boundary conditions, developed separately by some users, e.g., waves2Foam [28] and IH-FOAM [29]. However, the official version of OpenFOAM is not natively available to calculate the sediment transport and the bed morphological change, and the third-party module developed by other users could not be open accessed. Thus, we must self-extend aforementioned functionalities in this study. Moreover, the Reynolds-averaged Navier-Stokes (RANS) model was adopted in this study because it could provide more preferable information for the time-dependent scour profiles [30,31].

The rest of this paper is organized as follows: The numerical methods including the hydrodynamic model, bed morphodynamic model, as well as corresponding boundary conditions and numerical schemes are introduced in Sec. 2. The model validation in view of the free surface elevation, the velocity, the suspended load transport, and the sandy beach profile change to show the robustness of the adopted model is shown in Sec. 3. Model applications including detailed analyses of beach profile change, wave breaking, and hydraulic jump are conducted in Sec. 4. A discussion on the transport volume of onshore sediment is given in Sec. 5. The main conclusions drawn from this study are given in Sec. 6.

2 Numerical Methods

2.1 Hydrodynamic Model. The three-dimensional RANS solver was used to simulate the unsteady and incompressible viscous fluids, and a second-order standard $k-\varepsilon$ turbulent model was chosen to close the set of RANS equation. Then, the modified VOF method was used to track the free surface. Detailed description of aforementioned equations could be found in Ref. [32].

Bed shear stress is a fundamental parameter, which links the flow conditions and the wave motion to sediment transport. Some of the bed shear stress formulations, such as wall function [33], friction based [34], turbulent viscosity based [35] and turbulent kinetic energy based [36], are available in the literature for the estimation of bed shear stress. In this paper, as inspired by the studies of Arzani et al. [37], the wall shear stress vector could be computed as

$$\tau = \tau_t - (\tau_t \cdot \mathbf{n})\mathbf{n} \tag{1}$$

where the wall traction is obtained as $\tau_t = \sigma \cdot \mathbf{n}$, $\mathbf{n}$ is the unit normal vector that is perpendicular to the bed surface, and σ is the stress tensor given by

$$\sigma = -p\delta_{ij} + 2\mu S_{ij} \tag{2}$$

The first term is the pressure-induced stress term, where p is the pressure and δ_{ij} is the Kronecker delta confirmed as 1 if $i=j$ and as 0 if $i \neq j$. The second term is the viscous stress term controlled by the bottom fluid motion, where μ is the molecular dynamic viscosity coefficient and S_{ij} is the strain rate defined as

$$S_{ij} = \frac{1}{2}\left(\frac{\partial u_i}{\partial x_j} + \frac{\partial u_j}{\partial x_i}\right) \tag{3}$$

where u is the fluid velocity in the Cartesian coordinates (i.e., x).

2.2 Bed Morphodynamic Model

2.2.1 Bed Load Transport. Many bed load transport formulas have been proposed, such as those by Smith and Mclean [38],

Rijn [39], and Soulsby and Whitehouse [40]. In the present work, the one proposed by Engelund and Fredsøe [41] is adopted.

$$q_b = \begin{cases} 18.74(\theta - \theta_c)(\theta^{0.5} - \theta_c^{0.5})\sqrt{Rgd_{50}}d_{50} & \text{if } \theta > \theta_c \\ 0 & \text{if } \theta < \theta_c \end{cases} \tag{4}$$

$$\theta = \frac{\tau}{\rho g R d_{50}} \tag{5}$$

$$R = \frac{\rho_{\text{sed}} - \rho}{\rho} \tag{6}$$

where q_b is the bed load transport rate per unit width, θ is the shields number, θ_c is the critical shields number, g is the gravitational acceleration, d_{50} is the median sand diameter, and R is the relative density of sediment.

$$\frac{\theta_c}{\theta_{co}} = \cos\beta + \frac{\sin\beta}{\tan\varphi} \tag{7}$$

Equation (7) proposed by Allen [42] indicates that the critical shields parameter is adjusted to a higher value for sediment moving up the slope (positive angle) and a lower value for sediment moving down the slope (negative slope). β is the slope angle between the sand bed and the horizontal plane and φ is the sediment angle of repose. θ_{co} is the threshold shields parameter that can be calculated [40] as

$$\theta_{co} = \frac{0.3}{1 + 1.2D_*} + 0.055[1 - \exp(-0.02D_*)] \tag{8}$$

D_* is the dimensionless sand size

$$D_* = \left(\frac{gR}{\nu^2}\right)^{1/3} d_{50} \tag{9}$$

The bedload transport rates in different directions are given by

$$q_{bi} = q_b \frac{\tau_i}{|\tau|} - C|q_b|\frac{\partial \eta}{\partial x_i} \tag{10}$$

where η is the bed elevation and C is the constant in the range of 1.5–2.3, which is used to reflect the slope effect on the sediment flux and is specified to be 1.5 in the present study inspired by the studies of Brørs [43] and Liu and García [44].

2.2.2 Suspended Load Transport. For the suspended load model, its governing equation is a classical convection–diffusion equation as follows:

$$\frac{\partial c}{\partial t} + \nabla \cdot \left(\mathbf{u} + w_s \frac{\mathbf{g}}{|g|}\right)c = \nabla \cdot \left(\frac{\nu_d}{\sigma_c}\nabla c\right) \tag{11}$$

where c is the volumetric concentration of the suspended sediment, $\mathbf{u}$ is the flow velocity field, w_s is the fall velocity of the sediment in still water, ν_d is the diffusivity of the sediment, which equals turbulence eddy viscosity ν_t, and σ_c is the turbulent Schmidt number relating eddy viscosity and sediment diffusivity, which is taken to be 0.8 in the present study inspired by the study of Liang et al. [30].

The following formula of settling velocity for natural sands in clear water is used in this study [40]:

$$w_{s0} = \frac{\nu}{d_{50}}[(10.36^2 + 1.049D_*^3)^{1/2} - 10.36] \tag{12}$$

Due to the interaction among the settling grains, the settling velocity normally decreases as the concentration of sediment increases. The reduction of w_{s0} due to high sediment concentration is considered using an empirical formula [45]

$$w_s = (1 - c)^{\varsigma} w_{so} \tag{13}$$

where ζ is a sand size of suspended load-related constant and is specified to be 5.0 in the present research according to the study of Liang et al. [30].

Considering the complicated interaction among wave, air, and sandy beach, the traditional advection–diffusion type equation needs to be updated. Comparing with the traditional equation (i.e., Eq. (11)), the additional volume fraction α term has been introduced in Eq. (14).

$$\frac{\partial c}{\partial t} + \nabla \cdot \left(\alpha\mathbf{u} + w_s \frac{\mathbf{g}}{|g|}\right)c = \nabla \cdot \left(\alpha\frac{\nu + \nu_d}{\sigma_c}\nabla c\right) \tag{14}$$

The rate of change and the term including w_s in Eq. (14) are multiplied by α. This ensures that sediment, which accidentally is left in the air phase, drops out immediately after entering it. Furthermore, the presence of ν in Eq. (14) is included for numerical stability. This stability problem occurs when ν_d becomes 0; hence, the inclusion of ν ensures locally the solution of an advection–diffusion problem rather than an advection problem, where the latter is harder to solve numerically [46].

2.2.3 Bed Morphological Updating. Bed elevation changes are based on the continuity of sediment. The Exner equation, which describes the sediment continuity, is

$$\frac{\partial z}{\partial t} = \frac{1}{1 - n}(-\nabla q_b + D - E) \tag{15}$$

where z is the bed elevation, n is the porosity of the bed, q_b is the bedload transport rate vector whose components are given by Eq. (10), D is the deposition rate, and E is the entrainment rate. The deposition rate D at the bed is

$$D = c_s w_s \tag{16}$$

where c_s is the sediment concentration very near to the bed. In the current model, the concentration at the nearest cell center is used.

The near-bed sediment concentration at a reference level Δ_b above the bed, which can also be regarded as the interface between the bed load layer and the suspended sediment domain, is calculated by the following empirical formula proposed by Rijn [47]:

$$c_b = \frac{0.015 d_{50} T^{1.5}}{\Delta_b D_*^{0.3}} \tag{17}$$

T is the nondimensional excess shear stress, which can be calculated as

$$T = \left(\frac{\mu_{sc}\tau}{\tau_{cr}} - 1\right)^{1.5} \tag{18}$$

where τ_{cr} is the critical shear stress and μ_{sc} is the effective shear stress coefficient which can be calculated as follows:

$$\mu_{sc} = \left(\frac{18lg(12h/\Delta_b)}{C_{90}}\right)^2 \tag{19}$$

where h is the water depth and C_{90} is the grain-related Chezy coefficient

$$C_{90} = 18lg\left(\frac{12h}{3d_{90}}\right) \tag{20}$$

where d_{90} equals to $1.5d_{50}$.

The model proposed by Rijn [47] was used to calculate the entrainment rate E. It shows the vertical concentration gradient and could be described as follows:

$$E = \frac{\nu + \nu_t}{\sigma_c} \cdot \nabla c \tag{21}$$

2.2.4 Mesh Deformation. The coupling between the hydrodynamic model and the morphodynamic model is achieved by

moving the computational mesh in such a way that the bottom mesh is conformal with the sediment bed. The mesh motion is based on the interpolation of the rate of bed elevation change from the faces to the vertices and solution of the Laplace equation for the mesh vertices motion as described in Ref. [48]. Meanwhile, in order to maintain the bed slopes not exceeding the sediment angle of repose, mass-conservative sand slide algorithm as shown in Ref. [49] is employed, by solving the Exner equation at both point P and its ith neighbor as follows:

$$\frac{(z_{bp}+\Delta z_{bp})-(z_{bi}+\Delta z_{bi})}{\Delta l_{pi}}=\tan\phi \tag{22}$$

where z_{bp} and z_{bi} are the bed elevations at point P and its ith neighbor, Δz_{bp} and Δz_{bi} are the corresponding corrections imposed to satisfy the angle of repose at point P and its ith neighbor, and Δl_{pi} is the horizontal distance between the two cell centers, respectively. Δz_{bp} and Δz_{bi} are obtained by balancing the mass between the bed cell P and its ith neighbor as follows:

$$A_{bp}\cdot\Delta z_{bp}-\sum_i A_{bi}\cdot\Delta z_{bi}=0 \tag{23}$$

where A_{bp} and A_{bi} are the projection of the bed cells P and its ith neighbor, respectively.

2.3 Boundary Conditions. Proper boundary condition is necessary for numerical models to reproduce main aspects of the physical experiments. In this study, the wave-absorbing boundary developed by Higuera et al. [29] was employed at the inlet and outlet of the domain. Importantly, for the inlet boundary, the expressions proposed by Lee et al. [50] for the free surface and velocity are shown as follows:

$$\eta=H\sec h^2\left[\sqrt{\frac{3H}{4h^3}}X\right] \tag{24}$$

$$\frac{u}{\sqrt{gh}}=\frac{\eta}{h}\left[1-\frac{1}{4}\frac{\eta}{h}+\frac{h}{3}\frac{h}{\eta}\left(1-\frac{3}{2}\frac{z^2}{h^2}\right)\frac{d^2\eta}{dX^2}\right] \tag{25}$$

$$\frac{w}{\sqrt{gh}}=\frac{-z}{h}\left[\left(1-\frac{1}{2}\frac{\eta}{h}\right)\frac{d\eta}{dX}+\frac{1}{3}h^2\left(1-\frac{1}{2}\frac{z^2}{h^2}\right)\frac{d^3\eta}{dX^3}\right] \tag{26}$$

where η is the free surface elevation, H is the wave height, h is the water depth, $X=x-ct$, $c=\sqrt{g(h+H)}$ is the wave celerity, and u and w are the velocities in the streamwise and vertical directions, respectively.

In addition, the top boundary conditions were set as free to the atmosphere of total pressure is set to zero. The sandy bed is described as a no-slip condition of $\mathbf{u}=0$ with zero normal gradient for pressure, and its vertical moving velocity is kept consistent with the velocity of bed elevation change. To reduce the computational cost, the symmetric boundary condition was utilized at the two side faces of the domain in view of the spanwise symmetric distribution.

2.4 Numerical Schemes. The 3D computational space was discretized using the finite volume method, and the time derivatives were addressed by the Euler scheme. The PIMPLE algorithm with a mixture between pressure implicit with the splitting of operators and semi-implicit method for pressure-linked equations was used for the pressure–velocity solver. The multidimensional universal limiter for explicit solution method was employed to maintain boundedness of the volume fraction. The Gauss linear scheme and the Gauss linear corrected scheme were selected for the gradient term and the Laplacian term, respectively. Other detailed implementation can be found in the OpenFOAM® User Guide. The bed load and suspended load in the sediment transport were solved separately. The bed load can be calculated by employing shear stress that was obtained from the flow solver. The suspended load equation is a convection–diffusion equation, and the sediment was transported passively by the flow field. The finite volume method was also used to solve this equation. After the sediment load was calculated, the Exner equation was solved to change the bed elevation. In fact, the Exner equation is a two-dimensional (2D) equation although the bed is in 3D space. Therefore, a finite area method was used to solve the problem of fluid information mapped from 3D to 2D.

3 Model Validation

3.1 Sand Slide for Sandy Beach With a Larger Bed Slope. To validate the sand slide model, we used a constant beach slope of 45 deg, assuming the sediment angle of repose is 30 deg. Figure 1 shows the 3D morphological changes of this sandy beach after employing the sand slide model, all the bed slope angles to be less than or equal to the angle of repose. This result shows that the sand slide model can work well when the bed slope angle exceeds the angle of repose.

3.2 Net Entrainment of Sediment From the Loose Sand Bed Into Suspension. The transport capacity of suspended load was examined by the net entrainment experiment of Rijn [51]. In this experiment, the loose sand bed was led by a section of rigid bed and the inlet water is free of sediment (see Fig. 2). The flow is steady and uniform with water depth of 0.25 m and mean velocity of 0.67 m/s. The representative suspended particle size is 0.2 mm, and the corresponding settling velocity is set to be 0.022 m/s. As suggested by Rijn [51] and Wu et al. [52], k_s is taken to be 0.01 m.

Structured mesh was employed to discretize the entire computational domain; the gird sizes were kept constant in the x-direction (0.002 m), the y-direction (0.002 m), and the z-direction (0.002 m). The time step was automatically adjusted during the

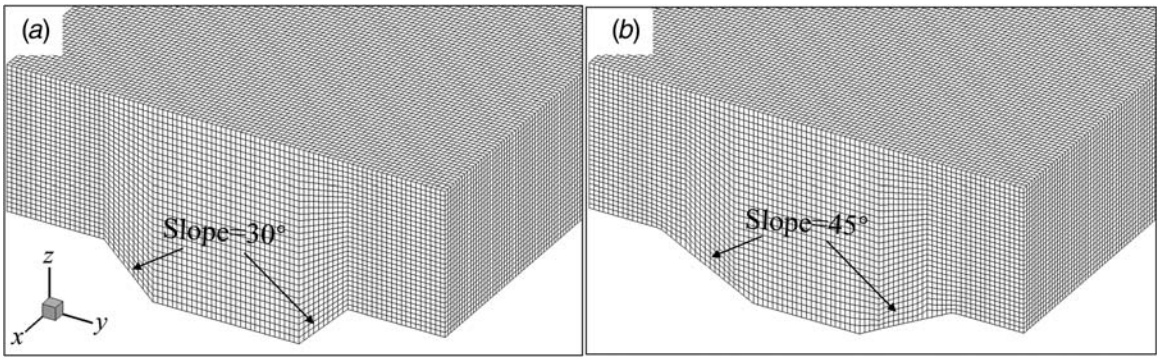

Fig. 1 Sandy beach profile: (*a*) before employing the sand slide model and (*b*) after employing the sand slide model

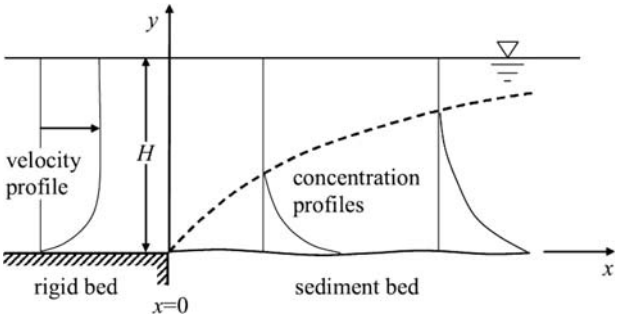

Fig. 2 Schematic view of the entrainment experiment

computation, ensuring that the Courant number c_r ($c_r = \Delta t \times \max(|\Delta u|)/\min(|\Delta x|)$, in which max ($|\Delta u|$) and min ($|\Delta x|$) were maximum velocity and minimum grid size, respectively, and Δt is the time step) was always less than one. To reveal model accuracy, a method presented by Willmott [53] was used in this study, which can be expressed as

$$\text{Skill} = 1 - \frac{\sum |X_{\text{model}} - X_{\text{exp}}|^2}{\sum \left(|X_{\text{model}} - \bar{X}_{\text{exp}}| + |X_{\text{exp}} - \bar{X}_{\text{exp}}|\right)^2} \tag{27}$$

where X is the variable and the overbar $\bar{X}$ denotes the mean of the variable. The perfect agreement between the model and the experiment will yield a skill of one and complete disagreement yields a skill of zero.

Figure 3 shows the comparisions of the experimental and numerical concentration distributions of suspended sediment at four typical locations at $x = 4H$, $10H$, $20H$, and $40H$. We could found that the suspended concentration of the inlet is zero for the clear water condition, and the sediment concentration decreases rapidly when the height from the bed surface increases which exhibits a parabolic profile. The model skill score in the selected position of 0.84, 0.92, 0.89, and 0.95 was computed. The higher value shows that the modeled result matches well with the experimental data.

3.3 Solitary Wave Runup on a Plane Beach. A typical case published by Synolakis [54] was abstracted to calibrate the robustness of the hydrodynamic transport process for the solitary wave propagating up a sloping beach. The beach slope is 1:19.85, water depth is 0.2885 m, and the wave amplitude to water depth ratio is 0.04. The solitary wave length is theoretically infinite. For practical use, its wave length L can be estimated as the distance that contains 95% of the total mass, namely, $L = 2.12h/\sqrt{H/h}$ [55], which is 3.06 m for this scenario ($h = 0.2885$ m and $H/h = 0.04$) that will be simulated in this study. Thus, we generated the numerical waves at 15 m upstream from the toe of the slope, which was sufficiently far. Meanwhile, we set the slope sufficiently long to guarantee that the maximum wave runup height on the slope cannot reach the outlet boundary of the domain.

In order to be consistent with the presentation in Ref. [53], the dimensionless time is defined as

$$T = \frac{t - t_0}{\sqrt{h/g}} \tag{28}$$

where t_0 is the arrival time of the wave front at the toe of the slope.

Figure 4 shows the comparisons of a sequence of the experimental and numerical wave profiles and the corresponding skill score. All skill values are more than 0.95 indicating the satisfactory agreements between the model and the experiment. Apart from acquiring the wave profiles, the experiments also quantitatively visualized the maximum runup height. The dimensionless maximum runup was predicted to be 0.151, which is very close to the measured value of 0.156 by Synolakis [54].

3.4 Beach Profile Change by the Solitary Wave. The transport capacity of water and sediment was also calibrated by the typical experiment conducted by Kobayashi and Lawrence [17]. The sandy beach slope is 1:12, sand particle is 0.18 mm, and porosity is 0.4. The experimental setup is shown in Fig. 5, and detailed

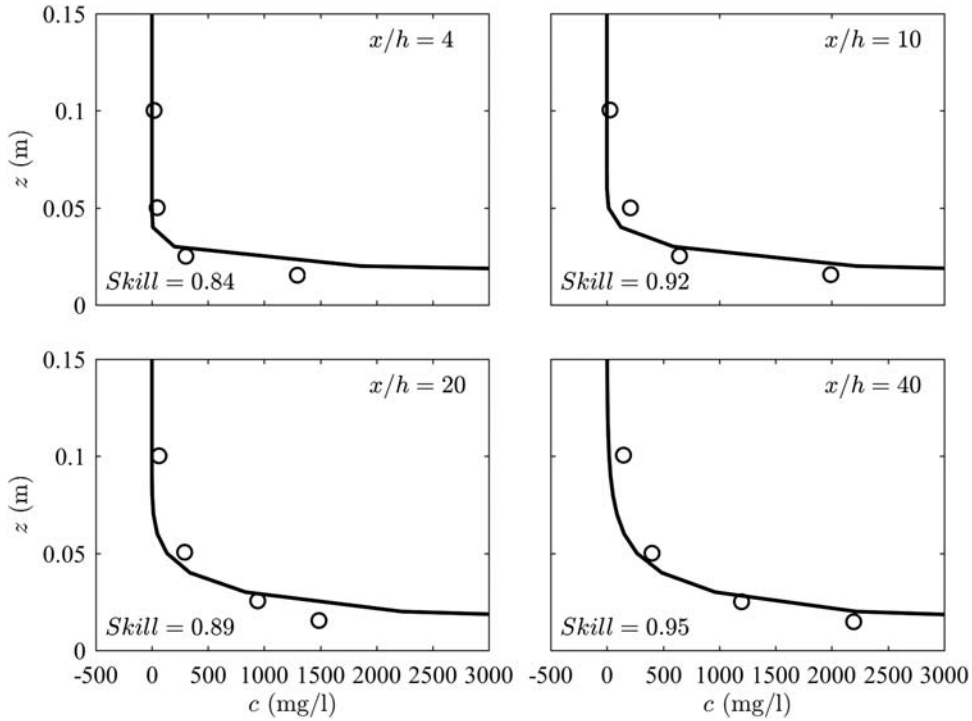

Fig. 3 Comparison of the predicted (solid lines) and measured (circles) sediment concentrations at four different locations

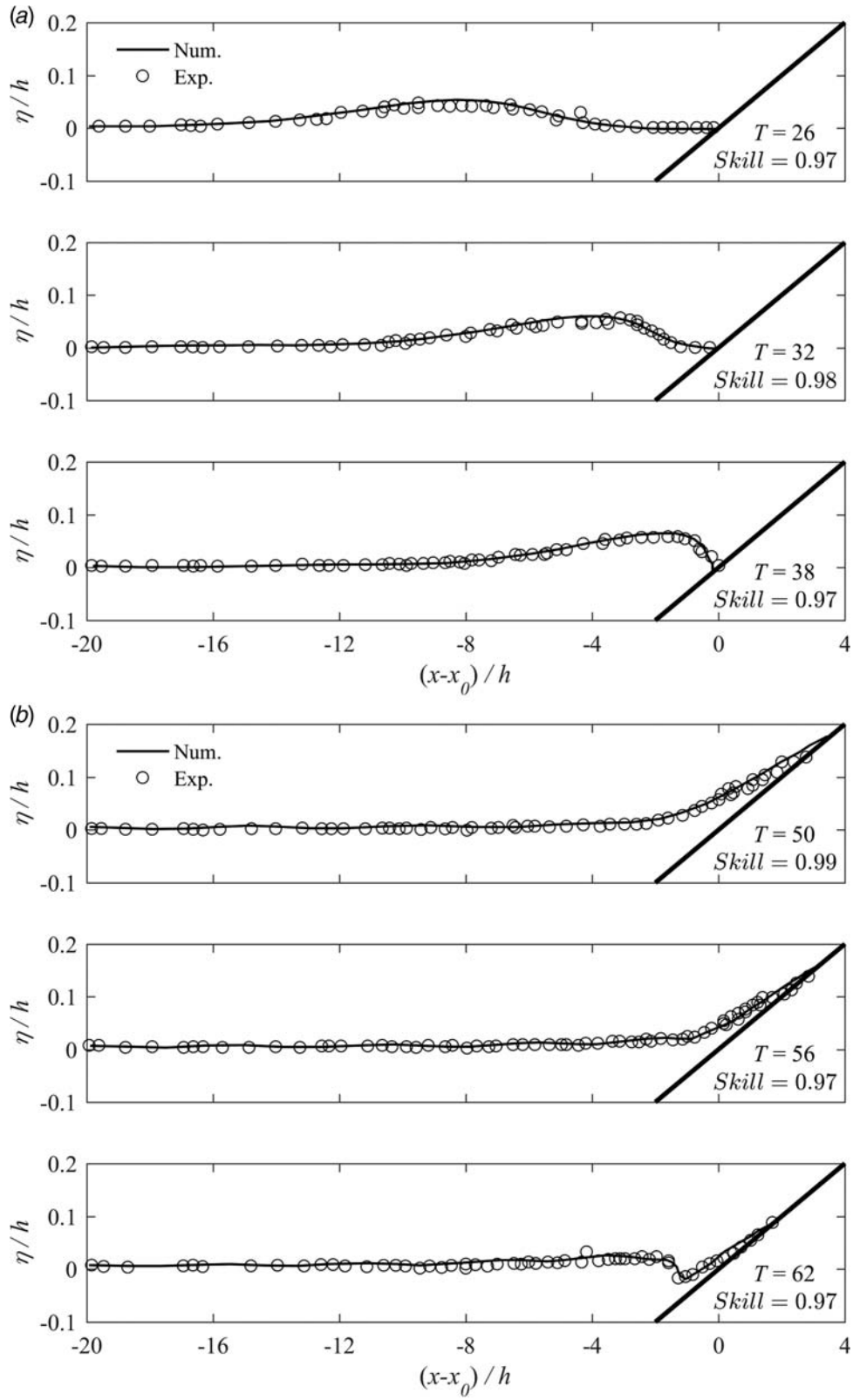

Fig. 4 Solitary wave transformation over a sandy slope: (*a*) runup and (*b*) drawdown

explanation of this experiment can be found in Ref. [17]. In the experiment, a solitary wave with water depth of 0.8 m and wave height of 0.216 m was first generated to propagate over the sandy beach. After this wave subsided, another solitary wave with the same height as the first one was generated on the evolved beach, and that cycle repeats. In this study, the experimental data of both the beach profile and the hydrodynamics change at the end of the fourth wave were selected.

Figure 6 shows a comparison of the water surface elevations on the evolving beach. As shown, the arrival times of the solitary wave show good agreement between the predicted results and the measured data. Moreover, all skill values are more than 0.7, the

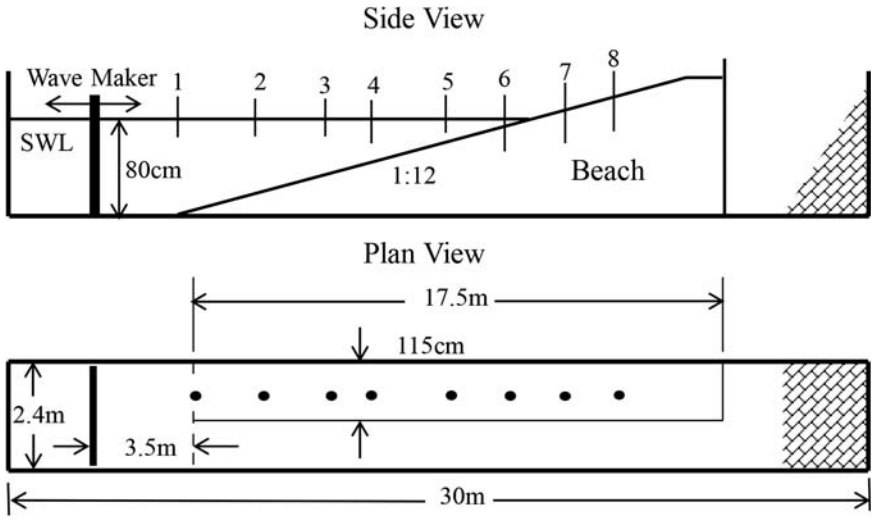

Fig. 5 Experimental setup for the beach profile change due to solitary waves

highest value is 0.96 and the average value is 0.85. The result shows that the predicted profiles of the solitary wave are in good agreement with the current model.

Figures 7(*a*) and 7(*b*) show a comparison of the beach profile and the beach profile change, respectively, and the corresponding skill value is 0.94. We can find that the predicted beach profile in the offshore and swash zones agrees well with the measured data. However, this model cannot accurately predict the measured beach profile around the coastline, especially $x = 10$ m. This may be due to the underestimation of the flow velocity induced by the backwash as will be introduced below, which attributed to the overestimation of the turbulent dissipation. Furthermore, the time series of normalized particle velocities at the acoustic Doppler velocimety (ADV) sampling location is shown in Fig. 7(*c*) for the streamwise component (u),

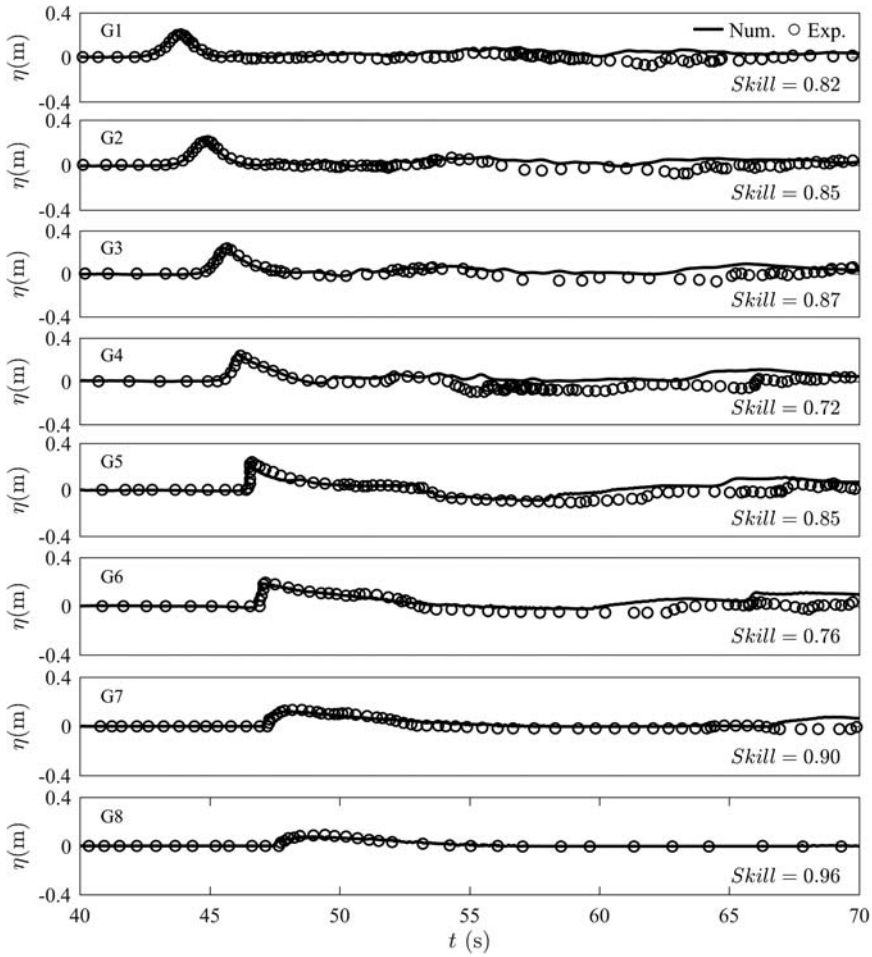

Fig. 6 Time series of the free surface elevations at the wave measurement locations

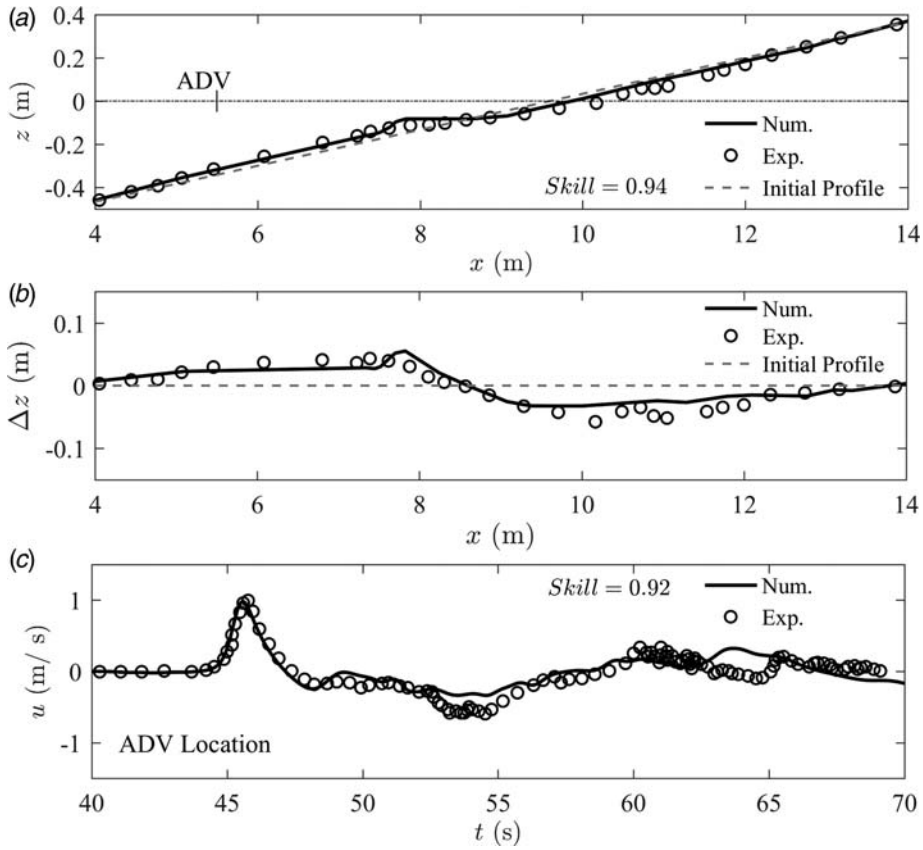

Fig. 7 The comparison of predicated results and measured data during the fourth wave for (*a*) beach profile, (*b*) beach profile change, and (c) time series of streamwise velocity (*u*) at the ADV location

and its skill value is 0.92. The numerical model satisfactorily reproduced the measurements for streamwise velocity associated with the leading solitary wave but underestimated the flow velocity induced by the backwash as mentioned. As a result, the proposed water-sediment transport model in this study could predict reasonably the reproduced beach profile change and associated hydrodynamic characteristics under the solitary waves, even though there are still some issues to be addressed in predicting the flow velocity during the backwash and the resulting beach profile change around the coastline.

4 Results

We have illustrated that the self-developed model is capable of modeling the breaking solitary wave propagation and the sediment transport on a sloping beach. In this section, we subsequently ran a couple of scenarios to state the water-sediment transport process and evaluate the effects of three factors (the incident wave height, the offshore water depth, and the beach slope) on the beach profile change and the sediment transport volume. In addition, the typical control factor related to the beach profile change during a tsunami-like solitary wave event will be clearly and rigorously recognized, and a dimensionless empirical equation will be proposed to predict the sediment transport volume. Four incident wave heights ($H = 0.2$m, 0.4m, 0.6m, and 0.8m), four water depths ($h = 1.5$m, 2m, 2.5m, and 3m), and four beach slopes ($m = 1{:}10$, 1:15, 1:20, and 1:25) were tested. In each scenario, we only changed one factor while keeping other three factors unaltered; thus, totally 12 scenarios were examined.

4.1 Process of the Beach Profile Change. Figure 8 shows the 3D mesh deformation due to the beach profile change, and the corresponding wave field and suspended load transport during the first solitary wave predicted for the typical case of $H = 0.8$m, $h = 2$m, and $m = 1{:}20$, in which Figs. 8(*a*)–8(*c*) are the runup processes and Figs. 8(*d*)–8(*f*) are the drawdown processes.

As shown in Fig. 8(*a*), the incident wave got steepened and skewed with the approach to the beach, and then, the solitary wave broke as a plunging breaker due to wave shoaling on the slope. At this moment, the fluid velocity at the upper part of the crest is larger than other fluid zone. Then, breaking wave impacting the local water near the coast, immediately developing a complex wave field with air entrainment on the free surface, but a weaker turbulence on the base of the wave due to the water depth sufficiently large, so that there is no obvious sediment suspension in Fig. 8(*b*). Subsequently, the broken wave-induced bore further runup, picking up amounts of sediment from the sandy beach into suspension by fluid momentum near the base of the wave. However, the beach profile change is not yet recognizable as indicated in Fig. 8(*c*), may be contributed to the wave-induced current direction opposite to the gravity of sediment and bottom friction. As a result, it is revealed that the beach profile is not affected by the flow velocity during wave runup, which was consistent with the measurements by Young et al. [20].

The drawdown process: A hydraulic jump was formed near the wave breaking region when the retreating water tongue collided with the relative still massive body of water as shown in Fig. 8(*d*). There was intensive sediment transport in the form of thick sheet flow on the landside of a hydraulic jump point. In this region, the drawdown flow velocity was high and the water depth was shallow with high sediment concentration, which resulted in net erosion of this region. As the water with high concentration of sediment was injected into the bottom of the hydraulic jump (Fig. 8(*e*)), a large recirculation region was formed that led to a turbulent hydraulic jump and roll. Meanwhile, the sediment suspension,

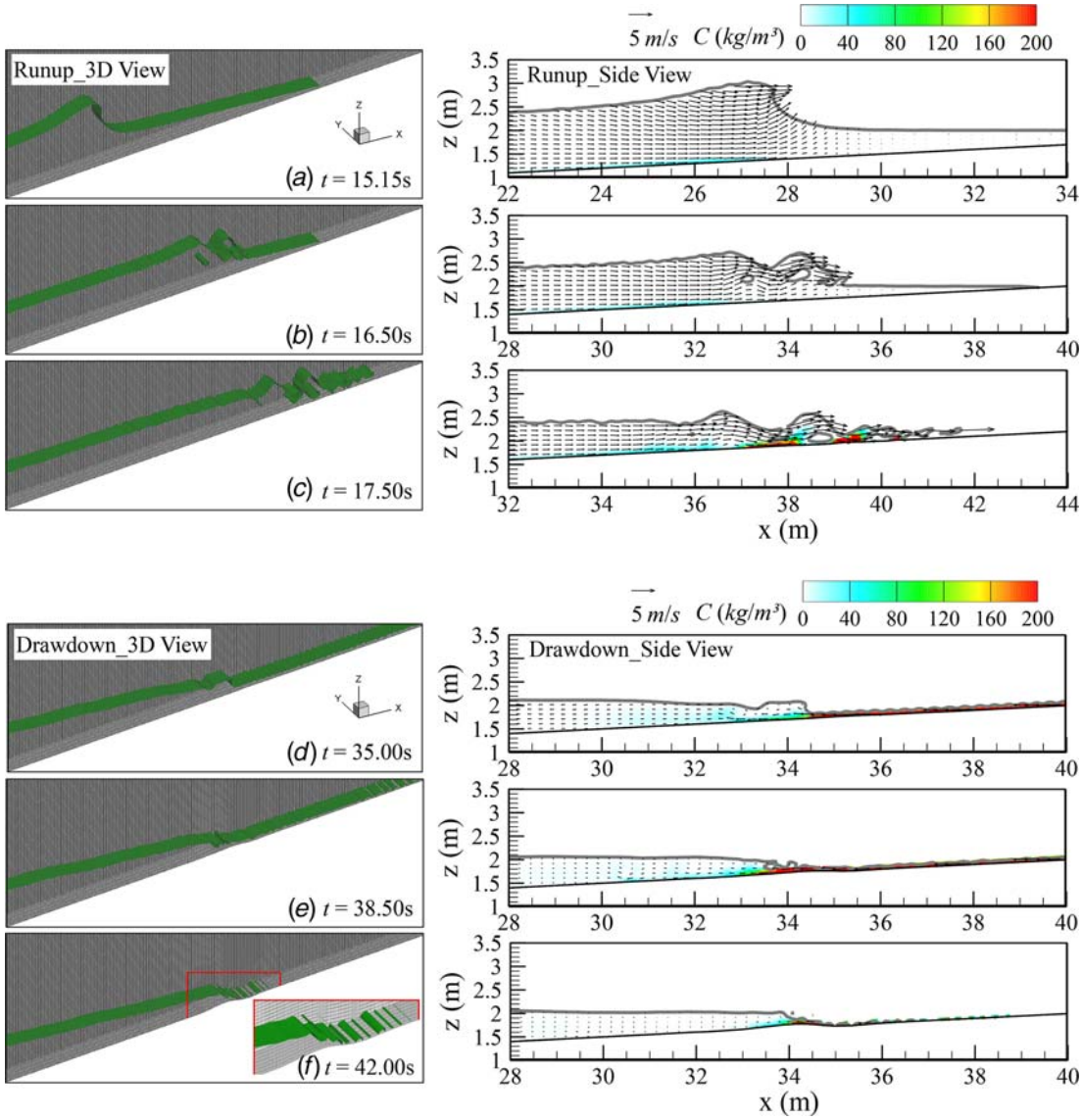

Fig. 8 (*a*)–(*c*) The 3D mesh deformation due to the beach profile change shown in the left panel, and the corresponding wave field and suspended load concentration shown in the right panel, during the solitary wave runup along the beach. (*d*)–(*f*) The 3D mesh deformation due to the beach profile change shown in the left panel, and the corresponding wave field and suspended load concentration shown in the right panel, during the solitary wave drawdown along the beach.

transport, and the erosion may be enhanced near the hydraulic jump zone. The sudden deceleration of the sediment-rich seaward flow, as well as the long particle residence time caused by the recirculation region, allowed the sediments to deposit in this region. Consequently, a large net deposit zone was observed in the recirculation region. At a later stage of the drawdown (Fig. 8(*f*)), the water supply of the retreating tongue decreased and was not enough to sustain the hydraulic jump, which thus weakened. Therefore, the hydraulic jump smoothed to become a wave-like pattern and propagated shoreward. Consequently, breaking solitary waves over a sloping sandy beach led to net erosion of the nearshore zone and net deposition in a seaward region of the hydraulic jump point. At this moment, the mesh deformation was obvious, and the figure was amplified partially to highlight this feature. The erosion and deposition patterns were consistent with the measurements of Kobayashi and Lawrence [17] and Young et al. [20].

4.2 Beach Profile Elevation Change. Figure 9 shows the morphological development for four different wave heights, and any one part figure shows the intermediate development, as well as the final profile for the entire simulation. We first found that the sand mass between erosion and deposition in the whole numerical domain is not seemed conserved. The difference value was calculated for the cases in Fig. 9 and found that the maximum value is less than 5% which may be attributed to the error accumulation from computational schemes [56]; thus, we believe that this inevitable lesser error should be accepted. We also found that the tsunami-like solitary wave led to the onshore erosion called the scour pit and offshore deposition called the sand bar below the still water surface. Following the impact time, the sand bar moves further to onshore, but the scour pit moves further to opposite direction. Meanwhile, the sand bar and the scour pit move to offshore as the wave height increased from $H = 0.2$ m to $H = 0.6$ m; however, aforementioned change is not obvious as the wave height further increased from $H = 0.6$ m to $H = 0.8$ m, and just found the onshore slope of the sand bar is steeper.

Figure 10 shows the morphological development for four different water depths. The beach profiles also exhibited the similar state with Fig. 9. The sand bar and the scour pit move to onshore as the water depth increased. The sandy beach response indicates that the

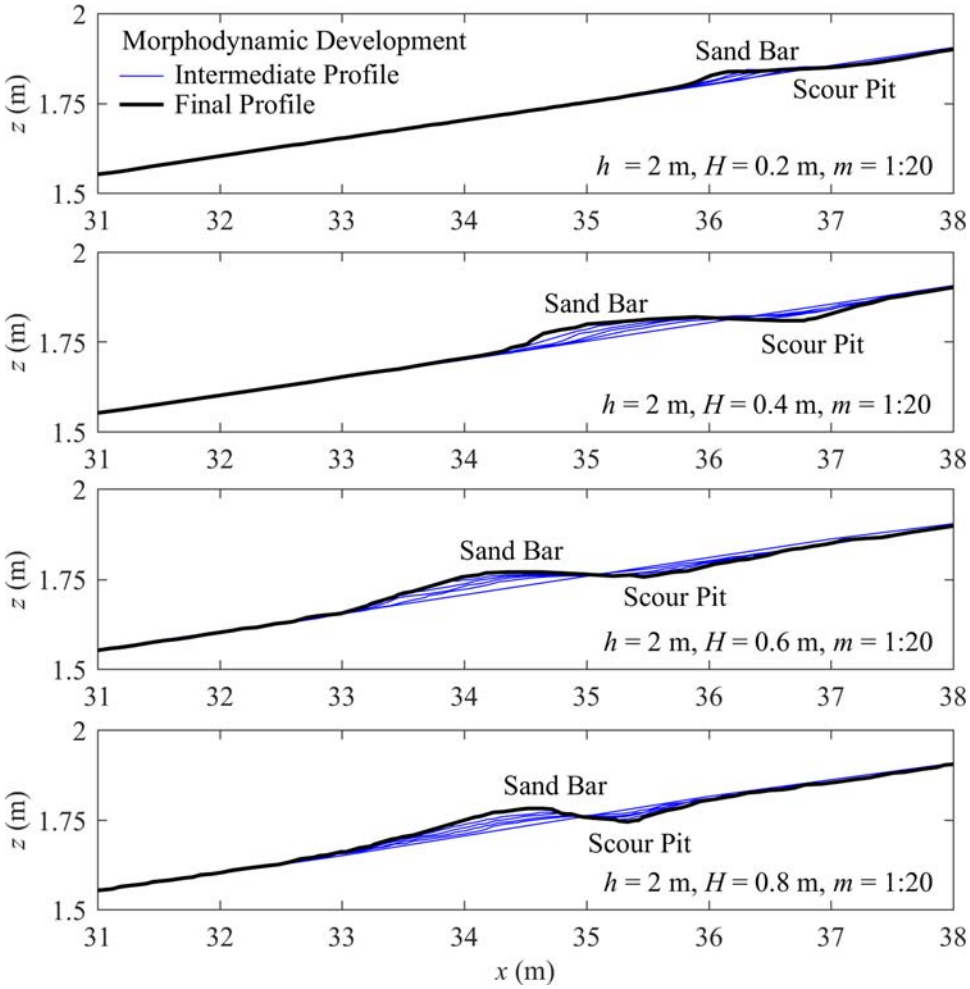

Fig. 9 The beach morphological development for four different wave heights

nearshore erosion will become more serious for the situation of mean sea level rise because of the greenhouse effect.

Figure 11 also shows the similar morphological development state for four different beach slopes, i.e., onshore erosion and offshore deposition. A prominent difference is found on the beach profile response to different beach slopes. The range of erosion and deposition is remarkable when the beach slope is larger (i.e., $m = 1{:}10$); this phenomenon mainly attributes to the larger active zone of the breaking wave and the larger gravity force component along sloping beach for the sediment particle. On the contrary, the beach profile response is not obvious when the beach slope trends to a smaller value (i.e., $m = 1{:}25$). Consequently, the case with the steeper slope is more susceptible to impacting failure.

4.3 Relationship Between the Hydrodynamic and the Beach Profile. Previous study revealed that the wave breaking [22] or hydraulic jump [20] could affect the beach profile change. To show the weight of the two hydrodynamic features on the beach profile change, a detailed analysis should be given. Figure 12 shows the variations of wave breaking and hydraulic jump with wave height. The breaking wave height increased with the increase of incident wave height, and the breaking wave point moves to offshore. However, the hydraulic jump occured in a narrow range at the location below the coastal line, and the hydraulic jump height also increased with the increase of incident wave height. In additon, we can find that the location and height of the hydraulic jump are kept similar for $H = 0.8$ m and $H = 0.6$ m. As shown in Fig. 9 for aforementioned two wave heights, the range of beach profile change and equilibrium location (i.e., the location of the beach profile is neither erosion nor deposition between the sand bar and the scour pit) is also kept consistent.

Figure 13 shows the variations of wave breaking and hydraulic jump with water depth. No obvious difference of the breaking wave height was found for different water depths, and the horizontal distance between the breaking wave point and the sandy beach is almost equal. As the water depth decreased, the hydraulic jump height and the sheet flow thickness decreased, correspondingly may induce the range of sediment transport for $h = 0.15$ m less than other cases with larger water depth, as indicated in Fig. 10.

Figure 14 shows the variations of wave breaking and hydraulic jump with beach slope. It is found that wave breaking was nearby the sandy beach for the larger beach slope, thus resulted intense sediment transport due to lesser wave energy loss. In addition, the hydraulic jump height shows a increased tendency with the increase of beach slope. This is anticipated that the majority of sediments were entrained by the intense hydraulic jump in the drawdown process to deposit and induced massive sediment trasport in a wide region in Fig. 11 combined with larger gravity force component along the sloping beach for the sediment particle.

Based on the aforementioned result, Fig. 15 shows the relationship between the equilibrium location and the wave breaking point or the hydraulic jump point. Meanwhile, corresponding tendency lines have been given, as shown in Eqs. (29) and (30).

Tendency line for the wave breaking point

$$y = 0.8248x + 3.1583, \quad R^2 = 0.884 \tag{29}$$

Tendency line for the hydraulic jump point

$$y = 0.9917x + 0.0793, \quad R^2 = 0.999 \tag{30}$$

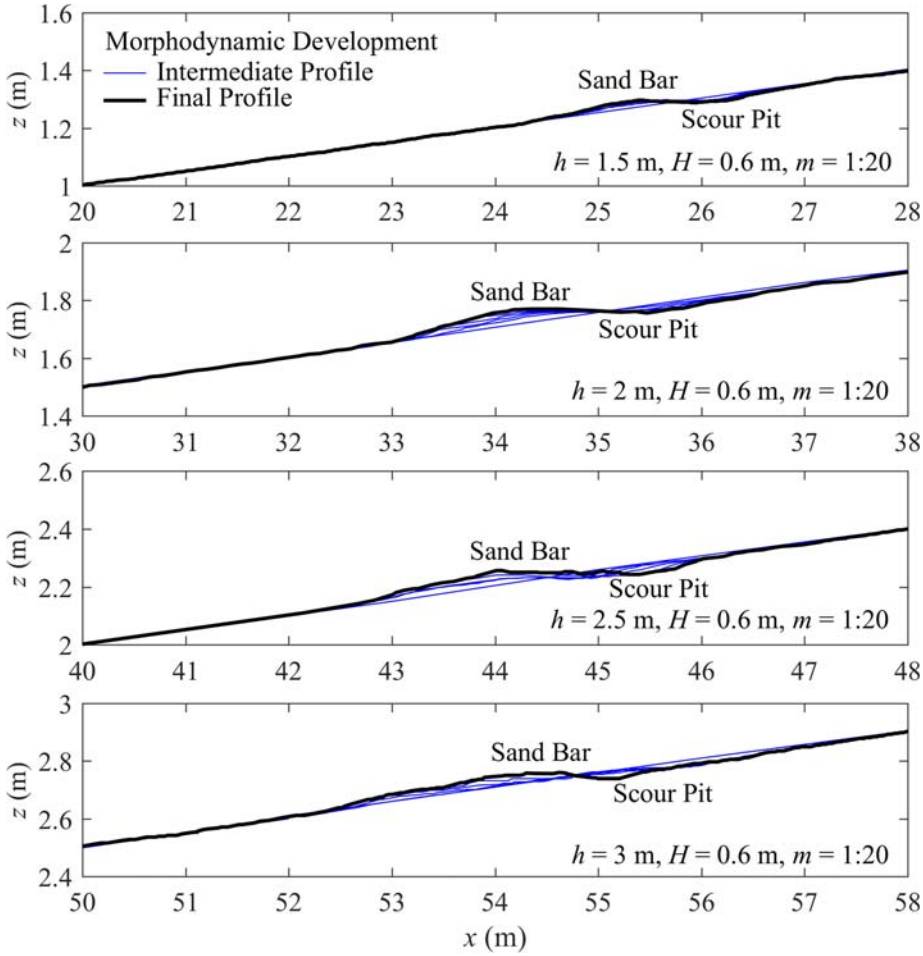

Fig. 10 The beach morphological development for four different water depths

The correlation coefficient between the hydraulic jump point and the equilibrium location is 99.9%, which is larger than that between the wave breaking point and the equilibrium location. It indicates that the hydraulic jump is more appropriate to describe the sediment transport comparison with the breaking point.

5 Discussion

As mentioned, incident waves are considerably effective in sediment transport as accuracy prediction of the transported sediment volume is one of the most important step to estimate the beach morphological development. The transported sediment volume per unit width (V_s) can be obtained by integrating the sandy beach elevation over the profile change. Figures 16(*a*)–16(*c*) show the variation of dimensionless transported sediment volume (V_s/H^2) for all aforementioned three factors (i.e., wave height, water depth, and beach slope). We can found the V_s/H^2 increased with both increasing wave height and increasing water depth. This is anticipated since the incident wave energy increased with the increase of wave height or water depth. Similar increasing variation of V_s/H^2 with the increasing beach slope was also found, which is identical to the variation of the profile change in Fig. 11, as well as the steeper slope caused the incipient wave breaking further landward as shown in Fig. 14; thus, less wave energy was dissipated before it impacted the sandy beach.

According to aforementioned analysis, we found a strong dependence of transported sediment volume (V_s) on wave height (H), water depth (h), and beach slope (m). In addition, Daghighi et al. [22] pointed out that V_s is dependent upon many factors such as sand diameter (d_{50}), water density (ρ), sand density (ρ_{sed}), distance from the beach toe to the breaking wave point (X_b), and gravity acceleration (g). Following the aforementioned study, we found that the hydraulic jump point (X_h) is more appropriate to describe the sediment transport comparison with the breaking point. Thus, in this study, the hydraulic jump point will be employed to discuss the variation of the transported sediment volume instead of the breaking wave point. Extending the study of Daghighi et al. [22], Buckingham π theorem was used for computing sets of dimensionless parameters from all aforementioned factors to eliminate the scale effects

$$f(V_s, H, h, m, d_{50}, \rho, \rho_{sed}, X_h, g) = 0 \tag{31}$$

$$\pi_1 = \frac{V_s}{H^2}, \quad \pi_2 = \frac{h}{H}, \quad \pi_3 = \frac{d_{50}}{H}, \quad \pi_4 = m, \quad \pi_5 = \frac{\rho_{sed}}{\rho}, \quad \pi_6 = \frac{X_h}{H} \tag{32}$$

Thus, dimensionless transported sediment volume (V_s/H^2) can be considered as a function of five other dimensionless parameters

$$\frac{V_s}{H^2} = F\left(\frac{d_{50}\rho_{sed}X_h}{\rho h H} m\right) \tag{33}$$

In order to obtain F function, we proposed the following dimensionless empirical relationship for V_s/H^2 through the regression analysis of all the scenarios in Fig. 16:

$$\frac{V_s}{H^2} = 0.125 \frac{h^{17.46} d_{50}^{0.47} \rho^{2.08}}{H^{1.81} X_h^{16.12} \rho_{sed}^{2.08}} m^{16.93} \tag{34}$$

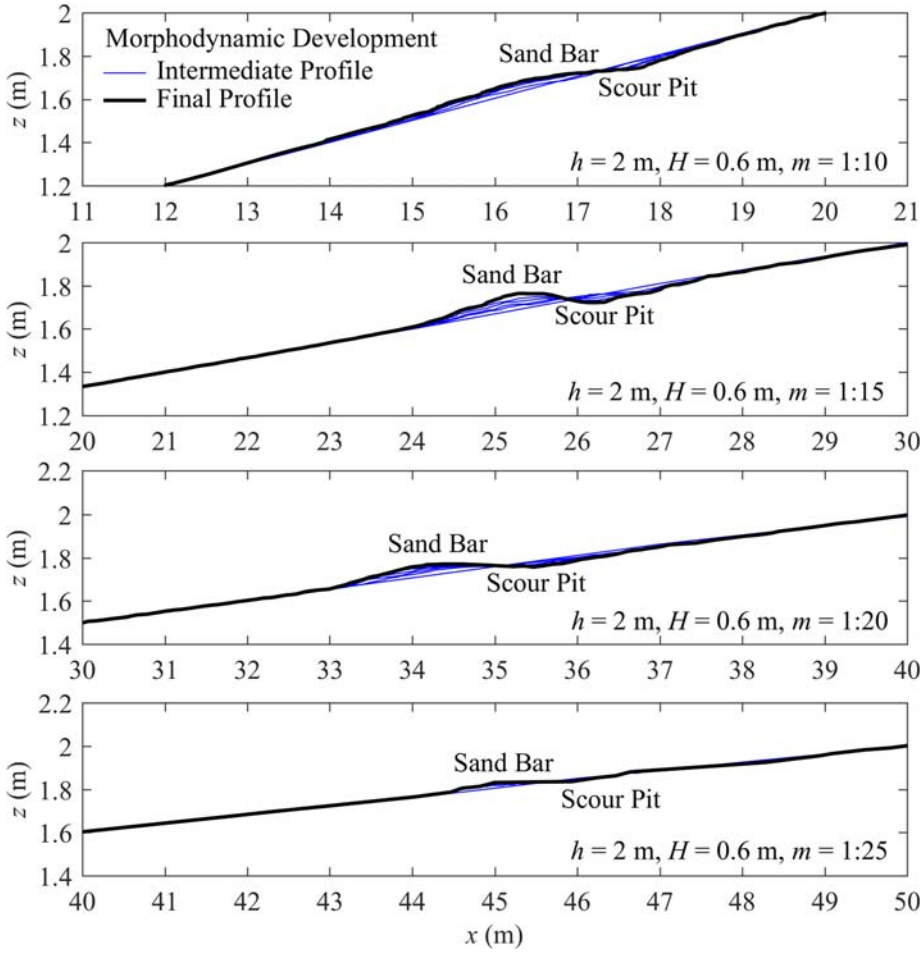

Fig. 11 The beach morphological development for four different beach slopes

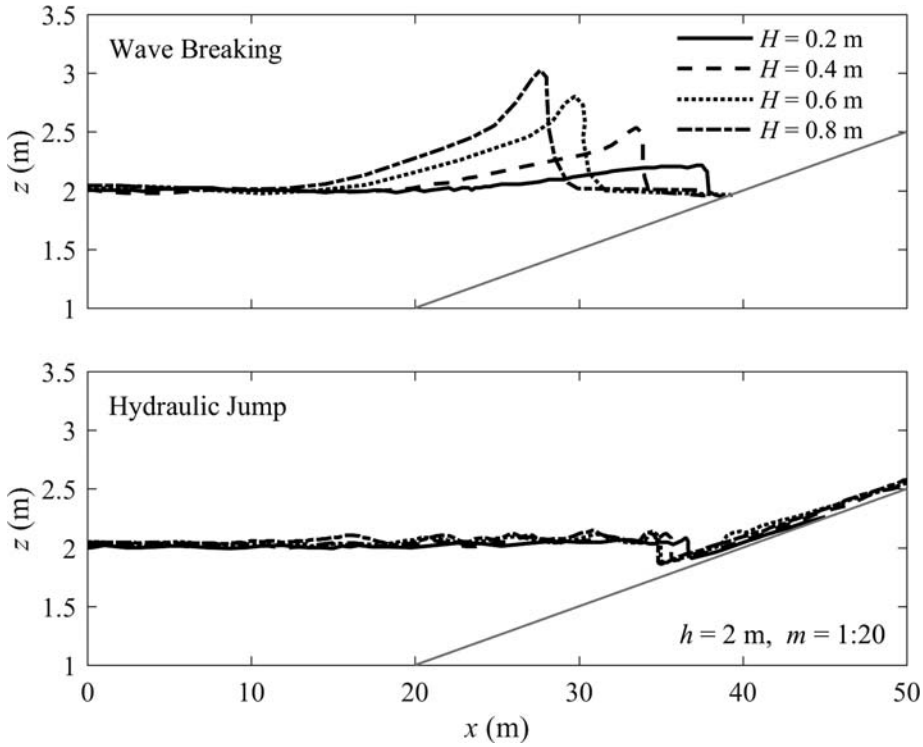

Fig. 12 Variations of wave breaking and hydraulic jump with wave height

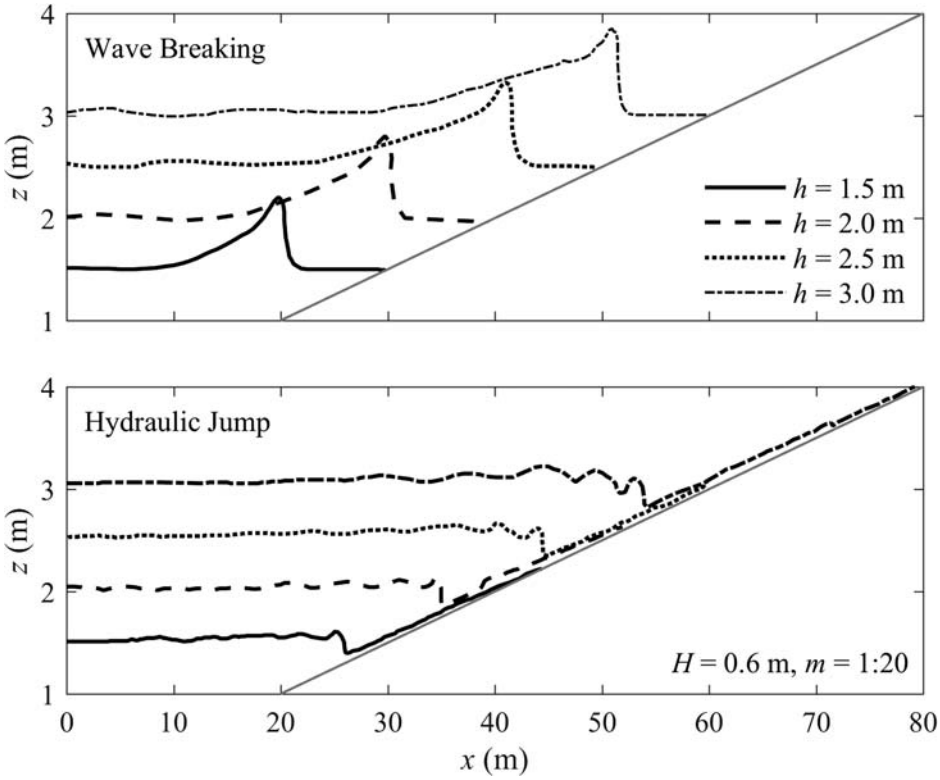

Fig. 13 Variations of wave breaking and hydraulic jump with water depth

The coefficient of determination R^2 is 0.95. Note that the above equation is valid for $0.1 \le H/h \le 0.4$, $1{:}25 \le m \le 1{:}10$, and fine sand within the tested range. Figure 17(*a*) compares the predicted V_s/H^2 with the computed V_s/H^2 based on the numerical simulations; a good agreement in the figure indicates the robustness of Eq. (34) to reproduce V_s/H^2 for the solitary wave interacting with a sloping beach. We additionally validated our formula subjected to the published data from Young et al. [20], Jiang et al. [21] and Daghighi et al. [22], in which the initial beach slope was exposed to a solitary wave one time, two times, and three times, respectively.

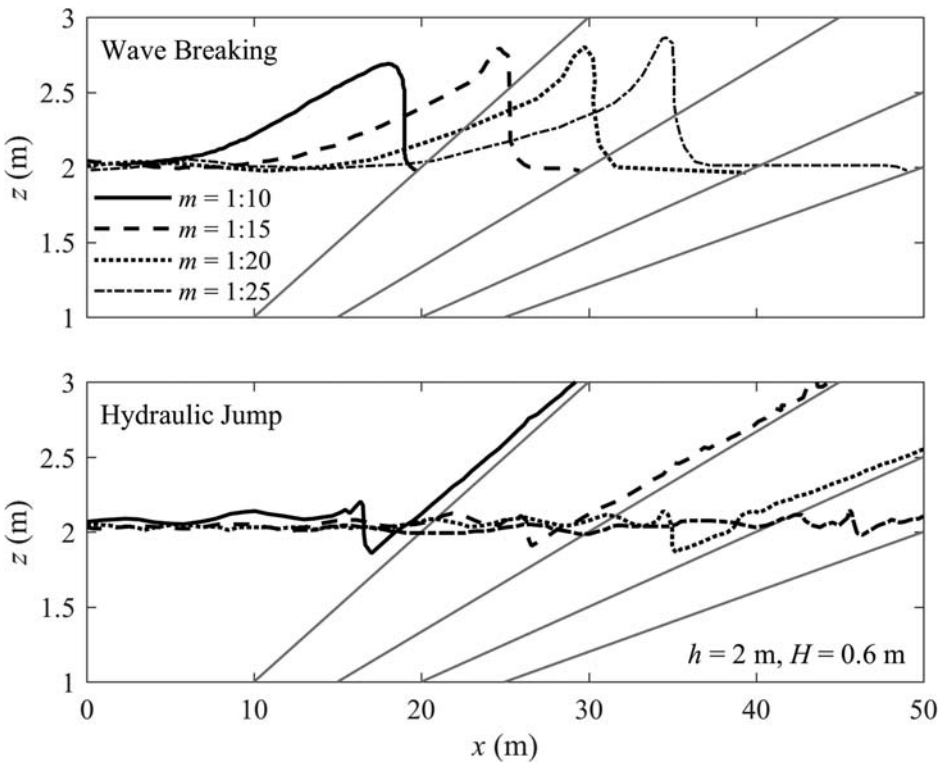

Fig. 14 Variations of wave breaking and hydraulic jump with beach slope

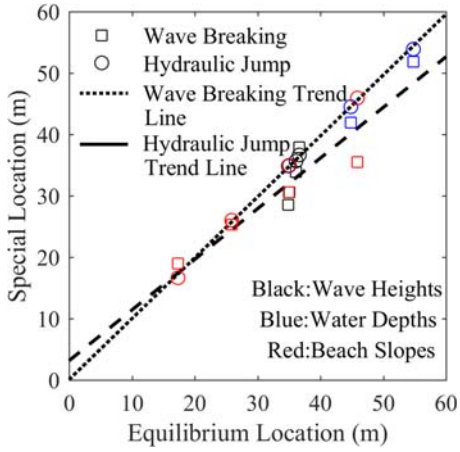

Fig. 15 The relationship between the equilibrium location and the wave breaking or the hydraulic jump

Satisfactory agreement between predicted V_s/H^2 and measured V_s/H^2 from Jiang et al. [21] could be found in Fig. 17(*b*). In addition, V_s/H^2 should be higher if the wave number increases, because the empirical relationship is acquired for the case of sandy beach exposed to a solitary wave one time in this study. Thus, our obtained values of V_s/H^2 are generally less than the values from Refs. [22,23]. We finally remark that when applying Eq. (34) to the prototype sandy beach, in addition to the factors explicitly included in Eq. (34), the angle of incident wave, debris, etc. might also affect the empirical values.

6 Conclusions

To remedy the deficiency of current understanding under a tsunami-like solitary wave in the water-sediment transport process, the beach profile change, and its typical control factor, as well as the sediment transport volume, a nonlinear 3D numerical sediment module was first self-developed based on Navier–Stokes equations in the OpenFOAM platform. The robustness of this model was validated by different published references.

The model was then applied to investigate the role of different factors (wave height, water depth, and beach slope) in affecting the beach profile change. A typical case was used to show the wave field, suspended load transport, and the resulting beach profile change during the first solitary wave. It is found that during the runup process, the sediments will be suspended by the breaking wave-induced turbulence movement at the near-bed region, and the suspended sediments subsequently pushed up the slope by fluid momentum. The sediment concentration is not obvious when the local breaking depth is larger. During the drawdown process, intense sediment transport was found in the form of rapid sheet flow, which leads to net onshore erosion and offshore deposition. It shows that the hydraulic jump point is more appropriate to describe the sediment transport comparison with the breaking point. Finally, the transport volume of onshore sediment was researched in detail, and we can found that larger wave height, water depth, and beach slope leaded to larger transport volume. Moreover, a dimensionless empirical equation considering multifactor was proposed to describe the transport volume of onshore sediment based on simulation results, and the corresponding proper parameters were recommended. This study will help to improve our understanding of the wave-induced sandy beach transport during the tsunami wave events.

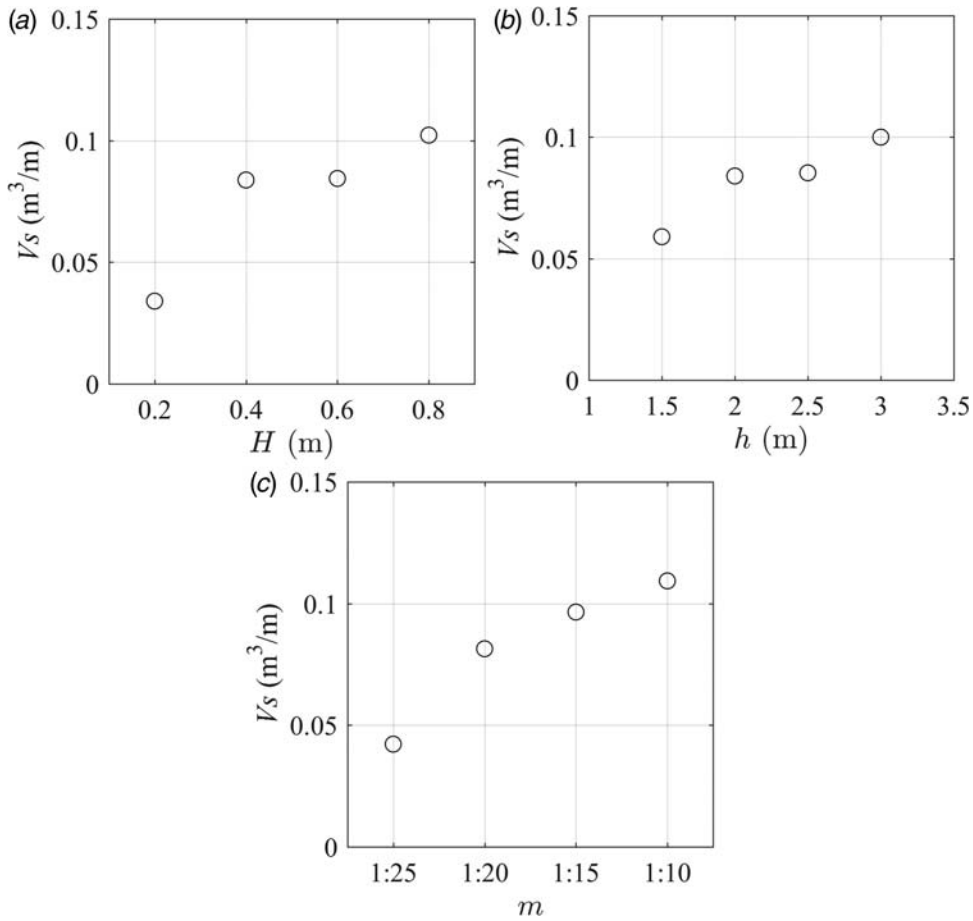

Fig. 16 Variations of dimensionless transported sediment volume (V_s/H^2) with (*a*) wave height (*H*), (*b*) water depth (*h*), and (c) beach slope (*m*)

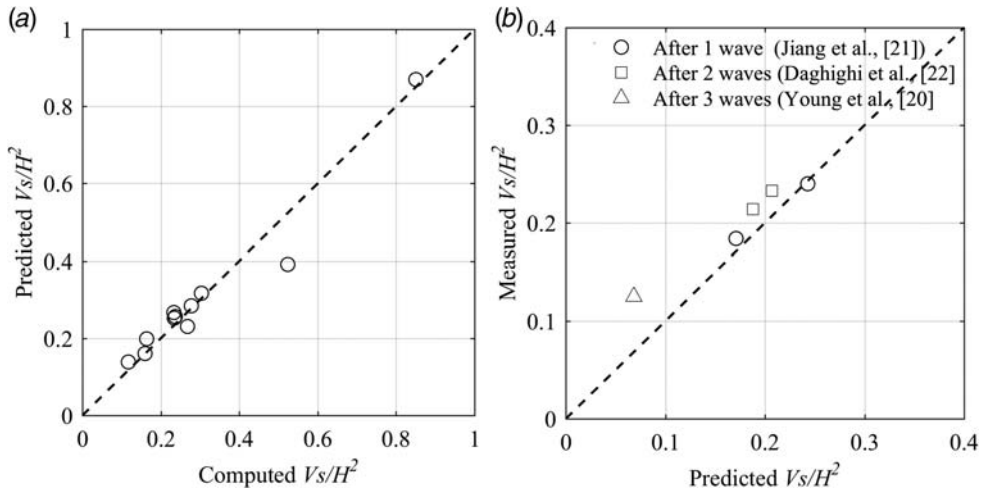

Fig. 17 (*a*) The computed dimensionless transported sediment volume (V_s/H^2) versus the predicted V_s/H^2 and (*b*) the predicted V_s/H^2 versus the measured V_s/H^2 from published references

The results obtained in this paper were based on the limited scale experiments. To eliminate the effect of scale, the model will need to be verified using field data or larger-scale laboratory experiments. In addition, the process of real tsunamis interaction with sandy beach is more complex than those modeled by physical and numerical experiments. Tsunami-induced currents and debris might also affect the hydrodynamic and morphological processes. Due to many uncertainties present in the nature water-sediment properties, therefore, this issue still needs further investigations. Nevertheless, the present numerical model provides an efficient tool to analyze more sophisticated problems, such as the scouring around the foundation of structures.

Funding Data

- National Natural Science Foundation of China (NNSFC) (Grant Nos. 51839002, 51879015, 51509023, 51809023, and 51779280).
- Guangdong Science and Technology Plan Program (Grant No. 2013B020200008).

References

[1] Titov, V., Rabinovich, A. B., Mofjeld, H. O., Thomson, R. E., and González, F. I., 2005, "The Global Reach of the 26 December 2004 Sumatra Tsunami," Science, **309**(5743), pp. 2045–2048.

[2] Mori, N., and Takahashi, T., 2012, "Nationwide Post Event Survey and Analysis of the 2011 Tohoku Earthquake Tsunami," Coastal Eng. J., **54**(1), pp. 1–27.

[3] Morton, R. A., Gelfenbaum, G., and Jaffe, B. E., 2007, "Physical Criteria for Distinguishing Sandy Tsunami and Storm Deposits Using Modern Examples," Sediment. Geol., **200**(3), pp. 184–207.

[4] Jaffe, B. E., Goto, K., Sugawara, D., Richmond, B., Fujino, S., and Nishimura, Y., 2012, "Flow Speed Estimated by Inverse Modeling of Sandy Tsunami Deposits: Results From the 11 March 2011 Tsunami on the Coastal Plain Near the Sendai Airport, Honshu, Japan," Sediment. Geol., **282**, pp. 90–109.

[5] Jaffe, B., Gelfenbaum, G., Rubin, D., Peters, R., Anima, R., Swensson, M., Olceses, D., Bernales, L., Gomez, J., and Riega, P., 2003, "Identification and Interpretation of Tsunami Deposits From the June 23, 2001 Perú Tsunami," Proceedings of International Conference on Coastal Sediments, Orlando, FL, pp. 1–13.

[6] Paris, R., Lavigne, F., Wassmer, P., and Sartohadi, J., 2007, "Coastal Sedimentation Associated With the December 26, 2004 Tsunami in Lhok Nga, West Banda Aceh (Sumatra, Indonesia)," Mar. Geol., **238**(1), pp. 93–106.

[7] Szczuciński, W., Kokociński, M., Rzeszewski, M., Chagué-Goff, C., Cachão, M., Goto, K., and Sugawara, D., 2012, "Sediment Sources and Sedimentation Processes of 2011 Tohoku-oki Tsunami Deposits on the Sendai Plain, Japan-Insights From Diatoms, Nannoliths and Grain Size Distribution," Sediment. Geol., **282**(1), pp. 40–56.

[8] Tzang, S. Y., Chen, Y. L., and Ou, S. H., 2011, "Experimental Investigations on Developments of Velocity Field Near Above a Sandy Bed During Regular Wave-Induced Fluidized Responses," Ocean Eng., **38**(7), pp. 868–877.

[9] Jiang, C., Wu, Z., Chen, J., Deng, B., Long, Y., and Li, L., 2017, "An Available Formula of the Sandy Beach State Induced by Plunging Waves," Acta Oceanol. Sin., **36**(9), pp. 91–100.

[10] Kobayashi, N., and Wurjanto, A., 1992, "Irregular Wave Setup and Run-Up on Beaches," J. Waterway Port, Coastal, Ocean Eng., **118**(4), pp. 368–386.

[11] Jacobsen, N. G., and Fredsoe, J., 2014, "Formation and Development of a Breaker Bar Under Regular Waves. Part 2: Sediment Transport and Morphology," Coastal Eng., **88**(3), pp. 55–68.

[12] Dean, R. G., 1991, "Equilibrium Beach Profile: Characteristics and Application," Coastal Res., **7**(1), pp. 53–84.

[13] Larson, M., Kraus, N. C., and Wise, R. A., 1999, "Equilibrium Beach Profiles Under Breaking and Non-Breaking Waves," Coastal Eng., **36**(1), pp. 59–85.

[14] Sénéchal, N., Dupuis, H., Bonneton, P., Howa, H., and Pedreros, R., 2001, "Observation of Irregular Wave Transformation in the Surf Zone Over a Gently Sloping Sandy Beach on the French Atlantic Coastline," Oceanol. Acta, **24**(6), pp. 545–556.

[15] Stark, N., "Pore Pressure Response to Irregular Waves at a Sandy Beach," Geotechnical Frontiers 2017, March 12–15, 2017, Orlando, FL, pp. 409–417.

[16] Lin, P., 2004, "A Numerical Study of Solitary Wave Interaction With Rectangular Obstacles," Coastal Eng., **51**(1), pp. 35–51.

[17] Kobayashi, N., and Lawrence, A. R., 2004, "Cross-Shore Sediment Transport Under Breaking Solitary Waves," J. Geophys. Res., **109**(C3), pp. 1–13.

[18] Moronkeji, A., and Rolla, O. H., "Physical Modelling of Tsunami Induced Sediment Transport and Scour," Proceedings of the 2007 Earthquake Engineering Symposium for Young Researchers, Seattle, WA, 2007, pp. 8–12.

[19] Tsujimoto, G., Kakinoki, T., and Yamada, F., 2008, "Time-Space Variation and Spectral Evolution of Sandy Beach Profiles Under Tsunami and Regular Waves," The Eighteenth International Offshore and Polar Engineering Conference, International Society of Offshore and Polar Engineers, Vancouver, Canada, pp. 1–5.

[20] Young, Y. L., Xiao, H., and Maddux, T., 2010, "Hydro- and Morpho-Dynamic Modeling of Breaking Solitary Waves Over a Fine Sand Beach. Part I: Experimental Study," Mar. Geol., **269**(3–4), pp. 107–118.

[21] Jiang, C., Chen, J., Yao, Y., Liu, J., and Deng, Y., 2015, "Study on Threshold Motion of Sediment and Bedload Transport by Tsunami Waves," Ocean Eng., **100**(1), pp. 97–106.

[22] Daghighi, N., Chegini, A. H. N., Daliri, M., and Hedayati, D., 2015, "Experimental Assessment of Sediment Transport and Bed Formation of Sandy Beaches by Tsunami Waves," Int. J. Environ. Res., **9**(3), pp. 795–804.

[23] Simpson, G., and Castelltort, S., 2006, "Coupled Model of Surface Water Flow, Sediment Transport and Morphological Evolution," Comput. Geosci., **32**(10), pp. 1600–1614.

[24] Pritchard, D., and Dickinson, L., 2008, "Modelling the Sedimentary Signature of Long Waves on Coasts: Implications for Tsunami Reconstruction," Sediment. Geol., **206**(1), pp. 42–57.

[25] Shimozono, T., Sato, S., and Tajima, Y., 2007, "Numerical Study of Tsunami Run-Up Over Erodible Sand Dunes," Sixth International Symposium on Coastal Engineering and Science of Coastal Sediment Process, New Orleans, LA, pp. 1089–1102.

[26] Xiao, H., Young, Y. L., and Prévost, J. H., 2010, "Hydro- and Morpho-Dynamic Modeling of Breaking Solitary Waves Over a Fine Sand Beach. Part II: Numerical Simulation," Mar. Geol., **269**(3), pp. 119–131.

[27] Nakamura, T., and Yim, S. C., 2011, "A Nonlinear Three-Dimensional Coupled Fluid-Sediment Interaction Model for Large Seabed Deformation," ASME J. Offshore Mech. Arct. Eng., **133**(3), p. 031103.

[28] Jacobsen, N. G., Fuhrman, D. R., and Fredsøe, J., 2012, "A Wave Generation Toolbox for the Open-Source CFD Library: OpenFoam®," Int. J. Numer. Methods Fluids, **70**(9), pp. 1073–1088.

[29] Higuera, P., Lara, J. L., and Losada, I. J., 2013, "Realistic Wave Generation and Active Wave Absorption for Navier–Stokes Models: Application to OpenFOAM®," Coastal Eng., **71**(1), pp. 102–118.

[30] Liang, D., Cheng, L., and Li, F., 2005, "Numerical Modeling of Flow and Scour Below a Pipeline in Currents: Part II. Scour Simulation," Coastal Eng., **52**(1), pp. 43–62.
[31] Jacobsen, N. G., and Fredsøe, J., 2011, "A Full Hydro- and Morphodynamic Description of Breaker Bar Development," Ph.D. thesis, Technical University of Denmark, Kongens Lyngby.
[32] Jiang, C. B., Liu, X. J., Yao, Y., Deng, B., and Chen, J., 2017, "Numerical Investigation of Tsunami-Like Solitary Wave Interaction With a Seawall," J. Earthq. Tsunami, **11**(1), pp. 1–18.
[33] Babaeyan-Koopaei, K., Ervine, D. A., Carling, P. A., and Cao, Z., 2002, "Velocity and Turbulence Measurements for Two Overbank Flow Events in River Severn," J. Hydraul. Eng., **128**(10), pp. 891–900.
[34] Schlichting, H., 1979, *Boundary-Layer Theory*, McGraw-Hill Book Company, New York.
[35] Zeng, J., Constantinescu, G., and Weber, L., 2005, "A Fully 3D Non-Hydrostatic Model for Prediction of Flow, Sediment Transport and Bed Morphology in Open Channels," Proceedings of the 31st IAHR Congress, Seoul, South Korea, pp. 1327–1338.
[36] Galperin, B., Kantha, L. H., Hassid, S., and Rosati, A., 1988, "A Quasi-Equilibrium Turbulent Energy Model for Geophysical Flows," J. Atmos. Sci., **45**(1), pp. 55–62.
[37] Arzani, A., Gambaruto, A. M., Chen, G., and Shadden, S. C., 2016, "Lagrangian Wall Shear Stress Structures and Near-Wall Transport in High-Schmidt-Number Aneurysmal Flows," J. Fluid Mech., **790**(1), pp. 158–172.
[38] Smith, J. D., and McLean, S. R., 1977, "Spatially Averaged Flow Over a Wavy Surface," J. Geophys. Res., **82**(12), pp. 1735–1746.
[39] Rijn, L. C. V., 1985, "Sediment Transport, Part I: Bed Load Transport," J. Hydraul. Eng., **110**(10), pp. 1431–1456.
[40] Soulsby, R. L., and Whitehouse, R. J. S. W., 1997, "Threshold of Sediment Motion in Coastal Environments," Pacific Coasts and Ports 1997 Conference, Christchurch, New Zealand, pp. 149–154.
[41] Engelund, F., and Fredsøe, J., 1976, "A Sediment Transport Model for Straight Alluvial Channels," Hydrol. Res., **7**(5), pp. 293–306.
[42] Allen, J. R. L., 1982, "Simple Models for the Shape and Symmetry of Tidal Sand Waves: (1) Statically Stable Equilibrium Forms," Mar. Geol., **48**(1), pp. 31–49.
[43] Brørs, B., 1999, "Numerical Modeling of Flow and Scour at Pipelines," J. Hydraul. Eng., **125**(5), pp. 511–523.
[44] Liu, X., and García, M. H., 2008, "Three-Dimensional Numerical Model With Free Water Surface and Mesh Deformation for Local Sediment Scour," J. Waterway Port, Coastal, Ocean Eng., **134**(4), pp. 203–217.
[45] Richardson, J. F., and Zaki, W. N., 1997, "Sedimentation and Fluidisation: Part I," Chem. Eng. Res. Des., **75**(1), pp. 82–100.
[46] Leveque, R. J., 2007, *Finite Volume Methods for Hyperbolic Problems*, Cambridge University Press, Cambridge.
[47] Rijn, L. C., 1984, "Sediment Transport, Part II: Suspended Load Transport," J. Hydraul. Eng., **110**(11), pp. 1613–1641.
[48] Jasak, H., and Tukovic, Z., 2006, "Automatic Mesh Motion for the Unstructured Finite Volume Method," Trans. FAMENA, **30**(2), pp. 1–20.
[49] Khosronejad, A., Kang, S., Borazjani, I., and Sotiropoulos, F., 2011, "Curvilinear Immersed Boundary Method for Simulating Coupled Flow and Bed Morphodynamic Interactions Due to Sediment Transport Phenomena," Adv. Water Resour., **34**(7), pp. 829–843.
[50] Lee, J. J., Skjelbreia, J. E., and Raichlen, F., 1982, "Measurement of Velocities in Solitary Waves," J. Waterway Port, Coastal, Ocean Div., **108**(2), pp. 200–218.
[51] Rijn, L. C., 1986, "Mathematical Modeling of Suspended Sediment in Nonuniform Flows," J. Hydraul. Eng., **112**(6), pp. 433–455.
[52] Wu, W., Rodi, W., and Wenka, T., 2000, "3D Numerical Modeling of Flow and Sediment Transport in Open Channels," J. Hydraul. Eng., **126**(1), pp. 4–15.
[53] Willmott, C. J., 1981, "On the Validation of Models," Phys. Geogr., **2**(2), pp. 184–194.
[54] Synolakis, C. E., 1987, "The Runup of Solitary Waves," J. Fluid Mech., **185**(1), pp. 523–545.
[55] Dean, R. G., and Dalrymple, R. A., 1991, "Water Wave Mechanics for Engineers and Scientists," *Advanced Series on Ocean Engineering 2*, World Scientific, Farrer Road.
[56] Jacobsen, N. G., 2015, "Mass Conservation in Computational Morphodynamics: Uniform Sediment and Infinite Availability," Int. J. Numer. Methods Fluids, **78**(4), pp. 233–256.